A cryogenic measurement setup for microelectromechanical systems used in space applications

Wen-Hsien Chuang, Thomas Luger, and Reza Ghodssi[a]
MEMS Sensors and Actuators Lab, Department of Electrical and Computer Engineering and the Institute for Systems Research, University of Maryland, College Park, Maryland 20742

Rainer K. Fettig
NASA Goddard Space Flight Center, Greenbelt, Maryland 20771

We present a cryogenic measurement setup installed inside a focused-ion-beam (FIB) system to characterize and microrepair microelectromechanical systems (MEMS) for space applications. The setup allows testing of MEMS devices under vacuum condition of 10^{-6} Torr at variable temperatures ranging from 298 to 20 K. In the experiment, a lead-zirconate-titanate translator powered by a function generator and a dc voltage is utilized as an actuator, and a thin-film thermo-resistor fabricated with test devices is used as an integrated temperature sensor. Additionally, a motorized *x-y-z* stage is installed to achieve highly accurate positioning function. Resonant techniques and bending tests based on the designed setup are developed to measure the mechanical properties of silicon nitride thin films at cryogenic temperatures. Combined with the functions of the FIB system, this setup also demonstrates the capability to microrepair microshutter arrays, programmable field selectors in the NASA James Webb Space Telescopes. The presented test setup exhibits its feasibility to test MEMS devices needed for the space applications and can be extended to other cryogenic applications. © *2005 American Institute of Physics.* [DOI: 10.1063/1.1884192]

I. INTRODUCTION

Microelectromechanical systems (MEMS) are micrometric devices which usually combine electrical and mechanical components, and are fabricated using integrated circuit batch-processing technologies. Various MEMS structures such as linear comb capacitors, micromirrors, microchannels, cantilevers, and diaphragms have been successfully fabricated and widely used in accelerometers, pressure sensors, optical switches, and lab-on-chip platforms. The advances of MEMS technologies also provide opportunities to develop MEMS devices for space applications. Due to the reduction of power and thermal requirements with miniature size and weight, microspacecrafts,[1] miniature communication satellites,[2] and meteorological instrumentation[3] have been proposed based on utilization of MEMS technologies. Currently, two-dimensional microshutter arrays are being developed at the NASA Goddard Space Flight Center (GSFC) to be used as programmable field selectors for a multi-object spectrometer on the James Webb Space Telescope (JWST).[4–6] The microshutter arrays, made of silicon nitride thin films using MEMS techniques, require cryogenic operation at 30 K to reduce thermal emission into the instrument. Since the JWST operates in outer space, making maintenance extremely complicated, a complete understanding of mechanical properties and reliability issues of MEMS materials and devices at cryogenic temperatures is critical for the development of the microshutter arrays.

The characterization of mechanical properties and reliability issues on the microscale is challenging due to the requirement of appropriate testing apparatus. Slight imprecision in the experimental setup, which has negligible consequences for macroscale measurements, can be a major source of systematic measurement errors for microsamples. In previous studies, several experimental setups and techniques were developed. A probe-based nanoindentation system[7] and an atomic force microscope[8] have been widely used to characterize mechanical properties and reliability issues of microsamples due to their high resolution measurement capability. Another approach is based on two-slit optical interferometry.[9] Instead of using two open slits, lithographically patterned gold strips on a microsample were utilized to reflect light. The distance between two gold strips can then be evaluated by examining the fringe patterns. However, all these testing apparatuses and techniques are only suitable for room-temperature measurement.

This article reports a cryogenic measurement setup installed inside a focused-ion-beam (FIB) system. We describe in detail the design, realization, and characterization of each component utilized in this setup. Finally, developed measurement techniques and capabilities based on the entire system are discussed.

II. SETUP DESIGN AND IMPLEMENTATION

The cryogenic measurement setup is designed to be installed inside a FEI-620 FIB system as shown in Fig. 1. FIB

---
[a] Author to whom correspondence should be addressed; present address: A. V. Williams Building, Room 1357, University of Maryland, College Park, MD 20742; electronic mail: ghodssi@eng.umd.edu
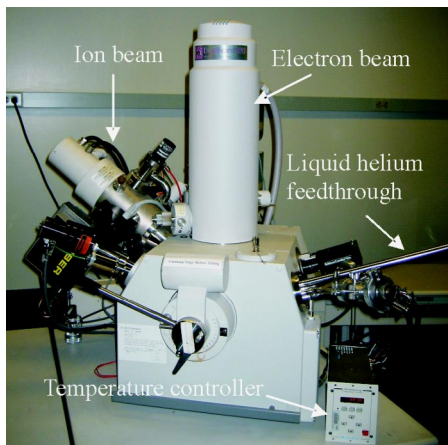
FIG. 1. FIB system with a cryogenic measurement setup installed inside. The helium transfer tube connecting liquid helium feedthrough and liquid helium Dewar is not shown in this figure.

systems have been widely used in the semiconductor industry to repair masks and interconnection wires, to provide maskless ion implantation, and to study failure mechanisms. The FEI-620 used in our experiments is a dual beam system, with ion and electron columns, permitting ion milling and *in situ* scanning electron microscopy (SEM). This system also has the ability to deposit platinum (Pt) by ion-induced metalorganic chemical vapor deposition. These unique capabilities make FIB an appropriate tool for characterizing mechanical properties and reliability issues of MEMS materials and devices at cryogenic temperatures.

Figure 2 shows the configuration of the cryogenic measurement setup inside the FIB system. Liquid helium (LHe) in combination with a resistive thermal source is used to
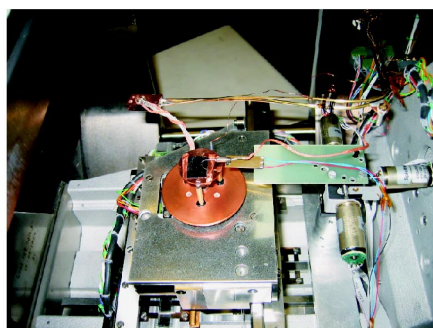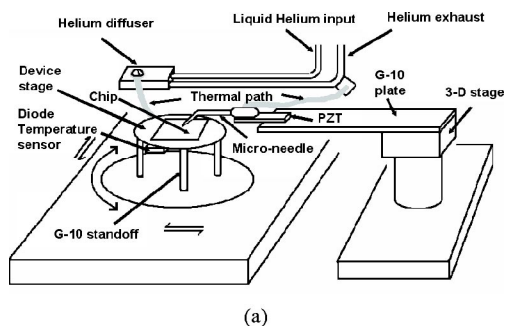

(a)

(b)

FIG. 2. Configuration of the cryogenic measurement setup inside the FIB system: (a) schematic view and (b) photograph of the system (shown without the Mylar shield for clarity).

control the temperature of the device stage by adjusting the flow rate of LHe and the electrical current flowing through the resistor. In order to transport LHe between a helium Dewar and the cryogenic measurement setup, a liquid helium feedthrough and a flexible helium transfer tube with multiple radiation shields and vacuum insulation are adopted.[10] Since the cryogenic measurement setup operates at temperature levels much below ambient temperature, heat transfer is the main concern when designing such a setup and, therefore, a thermally isolated device stage with cooling power is required. In our design, the cooling power is provided by a helium diffuser that is connected to a thermally isolated device stage (rotate-able and tilt-able) with a flexible wire providing a thermal path. Since copper has high thermal conductivity and can be machined easily, the device stage, the helium diffuser and the thermal path are made from copper. Three G-10 (a continuous filament glass cloth material with an epoxy resin binder) standoffs are used as thermal insulators (thermal conductivity of 0.04 W/m K at 30 K) to minimize conduction heat transfer between the device stage and the FIB chamber. Due to a high vacuum ($<10^{-6}$ Torr) inside the FIB system, convection heat transfer can be neglected. However, in most cryogenic setups, the primary mode of heat transfer is generally radiant heat transfer. In our design of the radiant shield, three layers of aluminized Mylar[11] enclosing the device stage are utilized to reduce radiant heat transfer due to the lower emissivity of aluminized Mylar compared with that of stainless steel/aluminum oxide chamber wall. Additionally, there is no thermal conduction path between the Mylar shield and the device stage.

A diode temperature sensor[12] attached to the device stage with thermal response time of 10 ms at 4.2 K and accuracy of 0.25 K at 30 K is first utilized to measure the temperature of the chip. The temperature reading and calibration are obtained from a temperature controller.[13] However, the temperature of a device chip may be different from the one measured by the diode temperature sensor due to thermal resistance between the device chip and the device stage. In addition, radiant heat transfer is not zero since the device stage is not wholly enclosed by aluminized Mylar layers. The opening is used for the entrance of electron and ion beams. To obtain an accurate temperature measurement, a temperature sensor integrated on the device chip is required.

There are several techniques used to design temperature sensors, such as the measurement of thermoelectric effect, thermomechanical effect, temperature dependence of electrical conductivity, and voltage-current (*V*-*I*) behaviors of diodes and transistors. In designing an integrated temperature sensor for our purpose, two issues need to be considered. First, the fabrication steps of this temperature sensor should be compatible with fabrication processes of the test devices. Second, the interconnection strategy should be simple. A thin-film thermo-resistor is adopted as an integrated temperature sensor and is shown in Fig. 3. A meander structure of the thermo-resistor is used to increase resistance value and sensitivity for temperature measurement. The interconnection is made using low-temperature conductive epoxy to connect the integrated temperature sensor with manganin wires.
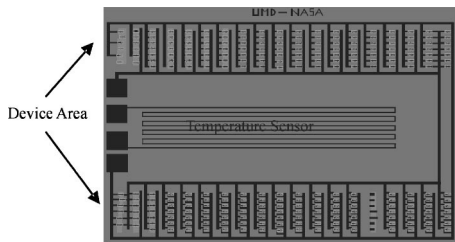
FIG. 3. Layout design of an integrated temperature sensor located in the center of a test chip. The area of the integrated temperature sensor is 5 mm × 10 mm.

Here, chromium/gold metallization with the thickness of 5 and 50 nm, respectively, is utilized as the structural layer for this thin-film thermo-resistor.

For actuating test devices and transporting membranes (discussed later), a lead zirconate titanate (PZT) translator powered by a function generator and a dc voltage is attached to a G-10 plate with a stycast epoxy.[14] The G-10 plate is then fixed on a three-dimensional (3D) stage controlled by three stepper motors. A small G-10 tube (10 mm in length, 3.5 mm in diameter, and 0.6 mm in wall thickness) with a thin metal layer at its inner surface is attached on the top surface of the PZT translator. A microneedle is mounted to the metal part at the end of this tube. A flexible copper wire (thermal path) cooling the microneedle is soldered to the metal part of the G-10 tube. This configuration prevents the PZT translator from malfunction as it remains warm during cryogenic operation of the microneedle.

III. SYSTEM CHARACTERIZATION

A copper block attached to the helium diffuser (Fig. 2) inside the FIB chamber is designed to calibrate the integrated temperature sensor as shown in Fig. 4. Both the diode temperature sensor and the integrated temperature sensor are placed and sit next to each other in this copper block. As copper is a good thermal conductor and FIB is a high vacuum system, the temperature difference between these two sensors is assumed to be negligible. During experiments, temperature is measured by the diode temperature sensor, while resistance is determined by the integrated temperature sensor. The relationship between temperature and resistance can be obtained (Fig. 5). From the measurement result, the
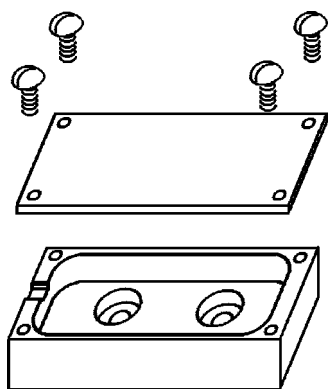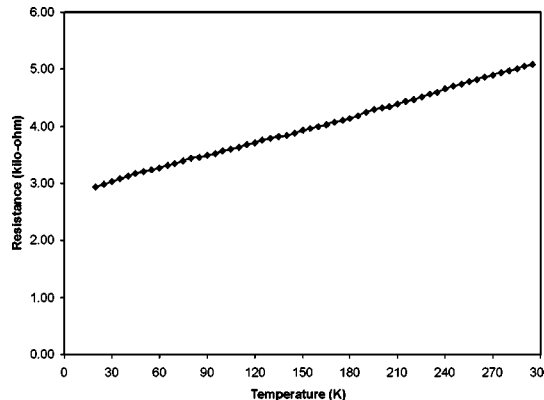

FIG. 5. Resistance-temperature curve of the integrated temperature sensor.

resistance of the integrated temperature sensor decreases linearly when cooling down to 20 K with an average sensitivity of 7.85 Ω/K, where no hysteresis of resistance is observed during the cooling and warm-up cycles (the difference is less than 1 Ω).

The calibrated integrated temperature sensor is then attached to the device stage as shown in Fig. 2. Two diode temperature sensors mentioned previously are utilized to monitor the temperatures of the device stage and the helium diffuser, respectively. When the temperature of the integrated temperature sensor (or the device chip) is set to 30 K by adjusting the flow rate of LHe, the temperatures of the device stage and the helium diffuser are found to be 22.6 and 4.2 K, respectively. The equivalent thermal model of the cryogenic measurement setup is presented in Fig. 6. Here, the values of 0.015 J/g K at 25 K, 0.0025 J/g K at 14.4 K, and 0.00015 J/g K at 4.2 K[15] are used as the specific heat of copper in the calculation of heat capacity. In addition, the temperature of the copper cable is assumed to be 13.4 K, the average value of the device stage and the helium diffuser.

IV. APPLICATIONS

A. Mechanical property measurement

A resonant technique based on the designed measurement setup is developed to determine the Young's modulus of silicon nitride thin films at cryogenic temperatures. T-shaped cantilevers are fabricated as testing structures using bulk micromachining technique.[16] Unlike conventional cantilevers, the T-shaped cantilever is formed by adding a mass (a square plate) at the end of a free-standing beam structure
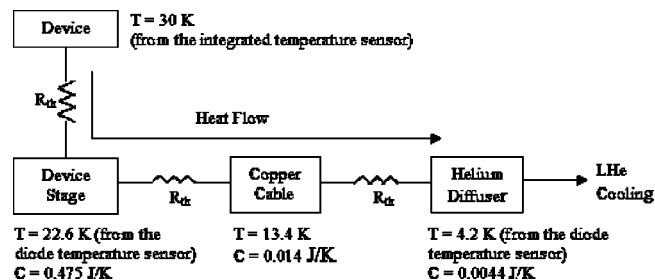

FIG. 4. Schematic view of the copper block for calibration of the integrated temperature sensor.

FIG. 6. Equivalent thermal model of the cryogenic measurement setup. Thermal capacity C and temperature T of each component are given at cryogenic temperatures. R_{th} represents thermal resistance.
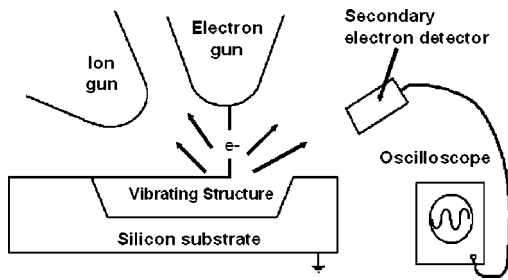
FIG. 7. Schematic diagram of the mechanism for the resonant test.

FIG. 9. Bending test of a T-shaped cantilever. The large blade of the cantilever is pushed by the microneedle until fracture.

to reduce its first resonant frequency. In our resonant tests, one T-shaped cantilever is first pushed vertically down with the microneedle and then released. The approximate resonant frequency is measured by pointing the electron beam in a fixed position where the vibrating T-shaped cantilever moves in and out of the electron beam path (Fig. 7). This modulates the secondary electron detector signal with the frequency of vibration. This signal is acquired with an oscilloscope and the approximate resonant frequency is determined. Subsequently, the microneedle driven by the PZT translator makes contact with the chip and vibrates the T-shaped cantilever near the frequency determined previously. The frequency is varied over a small range and the response is monitored to determine the exact resonant frequency and the quality factor. Figure 8 is a SEM picture illustrating that a T-shaped cantilever with a 52° titled angle vibrates only when the driving frequency of the PZT translator matches with its resonant frequency. Once the first resonant frequency is determined, the Young's modulus can be obtained by the following formula[17]

$$E = \frac{16\pi^2 f^2 L^4 \rho}{t^2}\left(\frac{w_b}{w_a}\frac{L_b}{L} + c_1\frac{L_a}{L}\right), \tag{1}$$

where f is the first resonant frequency in Hz, ρ is the mass density, L_a and w_a are the length and width of the cantilever beam, L_b and w_b are the length and width of the added mass at the end of the beam structure, $L=L_a+L_b/2$ is the effective cantilever length, c_1 is a constant (=0.2357), and t is the thickness.

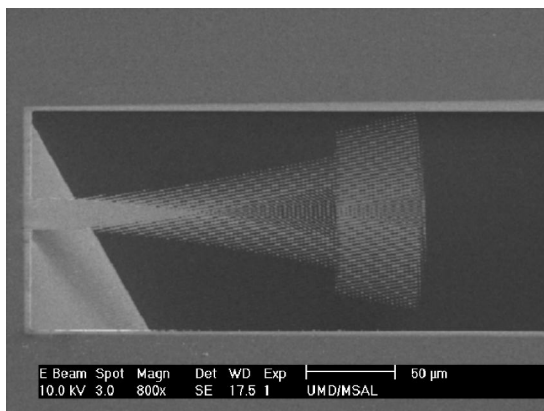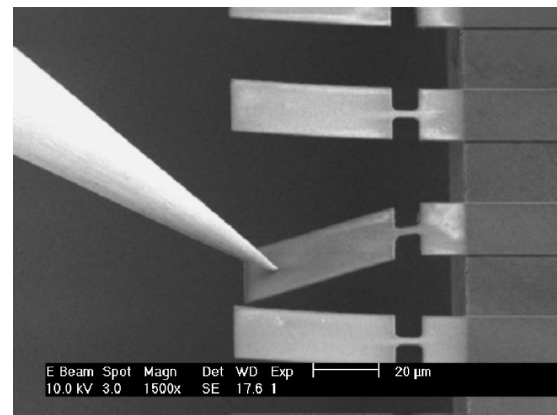For measuring the fracture strength of silicon nitride thin films at cryogenic temperatures, bending tests of T-shaped

cantilevers with different dimensional designs are performed. A large blade of a T-shaped cantilever is pushed by the microneedle through a rotation angle until fracture (Fig. 9). The bending angle before fracture is recorded and the fracture strength is then determined from ANSYS[TM] finite element simulation. The detailed analysis and testing results of the resonant technique and the bending tests can be found in our previous study.[18,19]

B. Microrepair of microshutter elements

The primary mission of the JWST is to reveal the origins of galaxies, clusters, and large-scale structures forming in the universe. In order to observe these faint galaxies, an object selector is needed for the operation of the JWST to increase instrument observing efficiency by optimally filling the focal plane without spectral overlap. A microshutter array with 1800×1800 elements to cover the JWST field of view is proposed and being fabricated at NASA GSFC.[4] Individual shutter elements consist of a shutter blade of low-stress low-pressure chemical vapor deposition (LPCVD) silicon nitride suspended from the shutter frame by a nitride torsion flexure. A schematic cross section of a single shutter element indicating the primary components is shown in Fig. 10. The shutter elements are normally closed and are opened by rotating 90° of the shutter blades, removing them from the optical beams. The key requirement of the microshutter array is to provide high on-to-off contrast ratio greater than 2000:1 at 30 K. However, the limitation of fabrication techniques makes the requirement difficult to achieve. Even though the microshutter array is fabricated using microfabrication techniques with a yield over 99%, in order to obtain such a high contrast ratio, broken elements in the array after fabrication must be blocked to keep them in the permanently closed state.

A technique to block a broken microshutter window at ambient temperature is developed using the cryogenic measurement setup and the FIB system. The microneedle is first placed in contact with an appropriate membrane which will

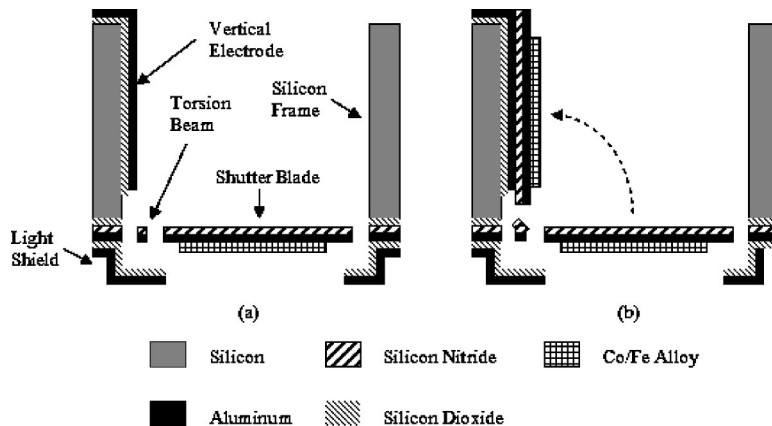FIG. 8. SEM picture of a T-shaped cantilever with a 52° titled angle at its first resonant mode.

FIG. 10. Schematic cross section of a single shutter element: (a) at close state, and (b) at open state.

be utilized to block the broken window. Here, we use the same shutter element as the membrane from a testing chip for this purpose. Ion-induced platinum deposition is performed to weld the microneedle to the membrane.[20] Next, the microneedle with the membrane is released as a free structure by using ion milling to separate the connection between the membrane and substrate. The microneedle with the membrane is positioned on a broken window, followed by ion-induced platinum deposition to weld the membrane to the broken window. Finally, the connection between the microneedle and the membrane is removed by ion milling. The experimental procedure is shown in Fig. 11. The microshutter devices in Fig. 11 are bonded to a chip carrier and only the front side (the side with a light shield) of each element

can be observed. In this experiment, the 3D stage and the PZT translator provide the freedom to move the microneedle with high resolution (a few nanometers). The optical test of the microshutter array with blocked windows has been performed, which shows promising results with one order of magnitude higher than the required contrast ratio. Further mechanical tests such as shock, vibration, and temperature cycling are currently under way to verify the reliability of this technique.

C. Stress balancing of multilayer structures

The microshutter arrays are optical MEMS devices operating in outer space. In order to prevent leakage light at the
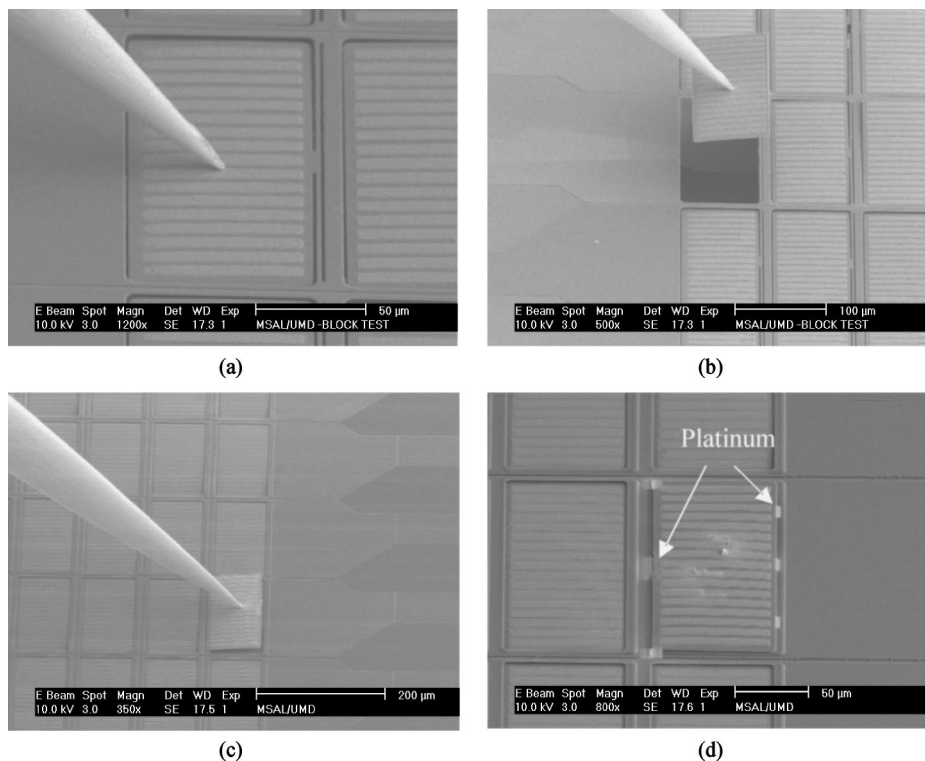

FIG. 11. Microrepair for blocking test of a microshutter array: (a) The microneedle is placed to contact a membrane utilized to block a broken shutter element. Ion-induced platinum deposition is then performed to weld the microneedle with the membrane. (b) The microneedle with the membrane is released by ion milling the connecting part of the membrane to the substrate. (c) Transport the membrane to the position of the broken shutter element. (d) The membrane is welded with the broken shutter window using platinum deposition. Finally, the microneedle is released from the membrane by ion milling.
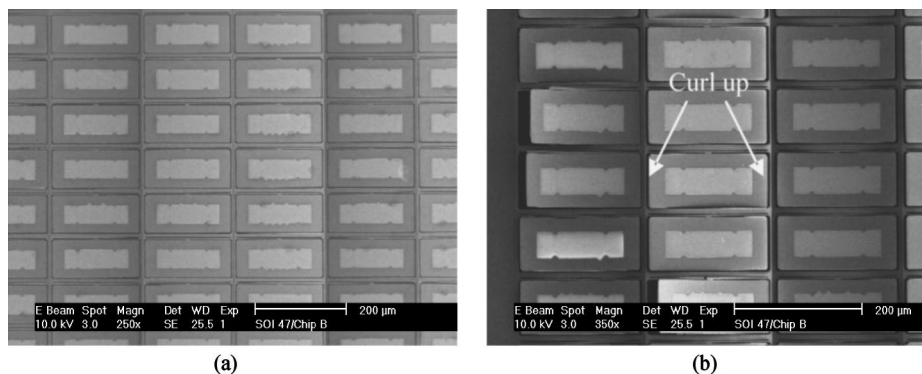
FIG. 12. SEM pictures of a microshutter array at (a) 298 K and (b) 30 K. The surface of the shutter element curls up at 30 K due to the mismatch of the coefficients of thermal expansion of the structural layers.

closed state of shutter elements, these devices require flat surfaces. As the structural layers of microshutter devices are low-stress LPCVD silicon nitride, aluminum, and cobalt/iron, the surfaces curl up 12 μm at 30 K due to the mismatch of the coefficients of thermal expansion (CTE) as shown in Fig. 12.

Since the residual stress of thin-film materials is sensitive to fabrication processes, one possible solution without dimensional modification of shutter elements is to tune parameters in microfabrication steps. The principle is to compensate the thermal stress with the induced residual stress at 30 K. The sputtering process of cobalt/iron deposition has been varied to obtain compressive residual stress and to intentionally curl down the shutter blade at room temperature as shown in Fig. 13. In this figure, the patterns of cobalt/iron are also modified as strip structures to prevent unwanted lateral movement of the shutter blades during magnetic actuation. However, when cooling down the microshutter arrays using the cryogenic measurement setup, the shutter elements still curl up 3.5 μm at 30 K as a result of insufficient thermal stress compensation. Further process tuning and development of a microstrain gauge for residual stress and CTE measurement are under investigation to achieve stress balance of these multilayer structures.
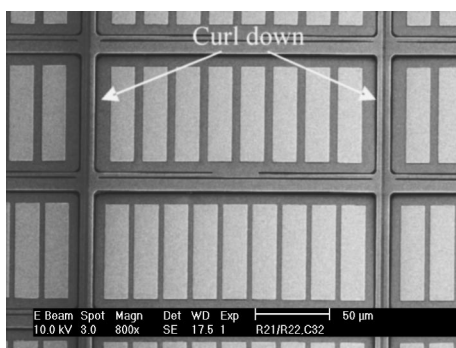

FIG. 13. SEM picture of a microshutter element with a curl-down surface at room temperature.

[1] T. K. Tang, Proc. IEEE International SOI conference, 67 (1999).
[2] S. J. Fiedziuszko, Proc. 13th International Conference on Microwaves, Radar, and Wireless Communications, 3, 201 (2000).
[3] D. Farrar, W. Schneider, R. Osiander, J. L. Champion, A. G. Darrin, and D. Douglas, Proc. Thermal and Thermalmechanical Phenomena in Electronic Systems, 1020 (2002).
[4] S. H. Moseley, R. K. Fettig, A. S. Kutyrev, C. Bowers, R. Kimble, J. Orloff, B. Woodgate, Proc. SPIE **3878**, 392 (1999).
[5] S. H. Moseley, R. K. Fettig, A. S. Kutyrev, M. J. Li, D. B. Mott, and B. Woodgate, Proc. SPIE **4178**, 51 (2000).
[6] M. J. Li, A. Bier, R. K. Fettig, D. Franz, R. Hu, T. King, A. S. Kutyrev, B. A. Lynch, S. H. Moseley, D. B. Mott, D. Rapchune, R. F. Silverberg, W. Smith, L. Wang, Y. Zheng, and C. Zinke, Proc. SPIE **4981**, 113 (2003).
[7] G. M. Pharr and W. C. Oliver, MRS Bull. **17**, 28 (1992).
[8] I. Chasiotis and W. Knauss, Proc. SPIE **3512**, 66 (1998).
[9] W. N. Sharpe, B. Yuan, and R. L. Edwards, J. Microelectromech. Syst. **6**, 193 (1997).
[10] Janis Research Company, Wilmington, MA, www.janis.com
[11] G. K. White and P. J. Meeson, *Experimental Techniques in Low-temperature Physics* (Oxford University Press, Oxford, 2002).
[12] Lake Shore Cryotronics Inc., Model: DT-470-SD-12, Westerville, OH, www.lakeshore.com
[13] Lake Shore Cryotronics Inc., Model: 321, Westerville, OH, www.lakeshore.com
[14] Lake Shore Cryotronics Inc., Stycast epoxy, Westerville, OH, www.lakeshore.com
[15] D. A. Wigley, *Mechanical Properties of Materials at Low Temperatures* (Plenum, New York, 1971).
[16] G. T. A. Kovacs, N. I. Maluf, and K. E. Peterson, Proc. IEEE **86**, 1536 (1998).
[17] W. D. Pilkey, *Formulas for Stress, Strain, and Structural Materials* (Wiley, New York 1994).
[18] W. H. Chuang, T. Luger, R. K. Fettig, and R. Ghodssi, J. Microelectromech. Syst. **13**, 870 (2004).
[19] W. H. Chuang, T. Luger, R. K. Fettig, and R. Ghodssi, Proc. of Material Research Society, 782, A5.21 (2004).
[20] W. H. Chuang, R. K. Fetting, and R. Ghodssi, Sensors and Actuators A, in press (2005).